Thin Solid Films 629 (2017) 60–68

Contents lists available at ScienceDirect

Thin Solid Films

journal homepage: www.elsevier.com/locate/tsf

Flash light sintering of ag mesh films for printed transparent conducting electrode

Chang-Jin Moon [a,b], Inyoung Kim [a,d,*], Sung-Jun Joo [b], Wan-Ho Chung [b], Taik-Min Lee [a,d], Hak-Sung Kim [b,c,**]

[a] Department of Printed Electronics, Korea Institute of Machinery and Materials (KIMM), 156 Gajeongbuk-ro, Daejeon, 34103, Republic of Korea
[b] Department of Mechanical Convergence Engineering, Hanyang University, Haengdang-dong, Seongdong-gu, Seoul 133-791, Republic of Korea
[c] Institute of Nano Science and Technology, Hanyang University, Seoul, 133-791, Republic of Korea
[d] Department of Nano Mechatronics, Korea University of Science and Technology (UST), 217 Gajeong-ro, Daejeon, 34113, Republic of Korea

ARTICLE INFO

Article history:
Received 11 October 2016
Received in revised form 2 March 2017
Accepted 25 March 2017
Available online 27 March 2017

Keywords:
Flash light sintering
Transparent conducting electrode
Reverse-offset printing
Ag mesh film

ABSTRACT

Transparent conducting electrodes (TCEs) are fabricated through the flash light sintering of reverse-offset printed Ag mesh patterns. Interestingly, the narrower printing lines require a higher flash light energy to obtain an equivalent sheet resistance even if the same Ag nanoparticle ink is used. The microstructural development of sintered Ag nanoparticles is also retarded with the decrease of line width after the same flash light sintering. The temperature calculation in the Ag mesh patterns clearly reveals that heat dissipation is affected by the print dimension. To improve the performance of Ag mesh TCEs with 3 μm wide lines, a preheating step comprised of multi-pulses is inserted before a main flash light sintering. The multi-pulsed flash light sintering is effective in decreasing the sample temperature and in removing the substrate damages or microstructural defects. As a result, the flash light-sintered Ag mesh TCEs shows a sheet resistance of 27 Ω/□ and an optical transmittance of 84.7% including an optical transmittance of substrate.

1. Introduction

Transparent conducting electrodes (TCEs) are a key component in various display and photovoltaic devices [1–6]. Indium tin oxide (ITO) has been mainly used for TCEs to satisfy both optical transparency and electrical conductivity in spite of the high cost that originates from the vacuum coating and photolithograph etching processes as well as the material scarcity of indium [7–10]. In recent years, as an alternative to ITO, printed metal mesh films have attracted substantial attention due to their practical advantages of having a simple process, which is composed of printing and sintering, and the ease in controlling sheet resistance and optical transparency by changing the design parameters [11–14]. Printing on a flexible polymer substrate can facilitate the introduction of a roll-to-roll(R2R)-based mass production system. Thus, besides metal mesh films, various solution-based materials, such as metal nanowires, graphene, and carbon nanotubes (CNTs) have been simultaneously adopted for electronic devices as ITO-free approaches [15–17]. However, post-heat treatment requires a temperature that is higher than the glass transition temperature (Tg) of conventional polymer substrates, which plays a technical obstacle for fabricating flexible TCEs on polymer substrates [18,19].

The flash light sintering technique has a remarkably fast sintering time that is compatible with the R2R-based printing speed [20–32]. In recent years, R2R-based photonic sintering has been carried out on flexo- or inkjet-printed silver nanoparticles by optimizing web speed, flash frequency, energy, and overlapping exposure areas [30–32]. Printed silver or copper films were converted to highly conductive electrodes after being exposed for only a few milliseconds at room temperature under an ambient condition and they showed excellent bending strength [33]. As a main mechanism of flash light sintering, it has been considered that the absorbed light energy through the plasmonic resonance of metal nanoparticles was converted to thermal energy [34,35]. The rapid increase of temperature inside printed films was monitored in real time during the flash light sintering process [28,36]. The side effects of surface cracks and film delamination were observed to originate from the abrupt evaporation of organic residues [28]. Two-step flash light sintering was suggested to remove microstructural defects and substrate warpage [27,28].

The conversion and release of thermal energy plays a critical role on the practical application of flash light sintering process but is still an unexplored field. In this study, we employed flash light sintering to the fabrication of printed silver mesh TCEs. We investigated the effect of print dimension on flash light sintering by analyzing the electrical and optical properties of printed Ag mesh patterns. The temperature

* Correspondence to: I. Kim, Department of Printed Electronics, Korea Institute of Machinery and Materials (KIMM), 156 Gajeongbuk-ro, Daejeon 34103, Republic of Korea.
** Correspondence to: H.S. Kim, Department of Mechanical Convergence Engineering, Hanyang University, Haengdang-dong, Seongdong-gu, Seoul 133-791, Republic of Korea.
E-mail addresses: ikim@kimm.re.kr (I. Kim), kima@hanyang.ac.kr (H.-S. Kim).

http://dx.doi.org/10.1016/j.tsf.2017.03.049
0040-6090/

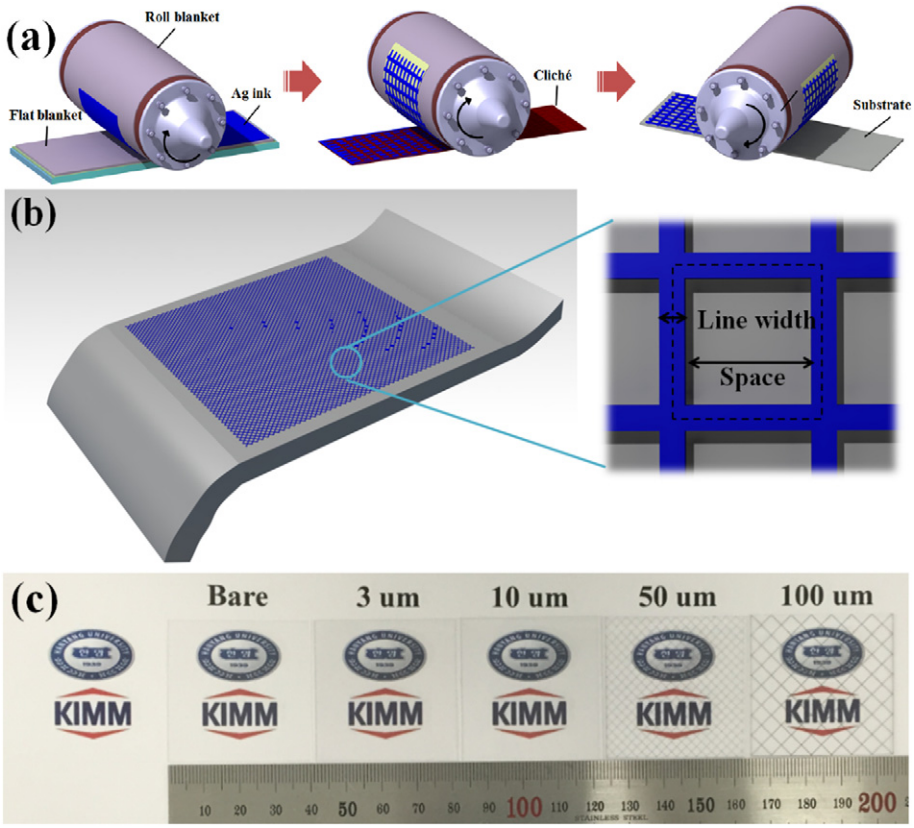

Fig. 1. Schematic diagrams of (a) reverse-offset printing and (b) Ag mesh film with design factors. (c) Optical images of printed Ag mesh film with different line widths.

changes that occurred during sintering were calculated by using a 2-D heat transfer model to understand the relationship between heat dissipation and print dimension. Based on our experimental results and calculations, we propose the use of the multi-pulsed flash light sintering process for finely printed silver mesh film for TCEs.

2. Experimental procedures

2.1. Reverse-offset printing of silver mesh patterns for TCEs

Commercial Ag nanoparticle ink (Silverjet DGP for reverse-offset, ANP Co.) is formulated with a solid content of 25 wt% and then stirred with a magnetic bar for one day. Using this nanoparticle ink, we reverse-offset printed Ag mesh patterns with different line widths on 180 μm thick polycarbonate (PC) films, as shown in Fig. 1 (a). First, the Ag ink was spin-coated on a flat blanket at a speed of 6000 rpm for 10 s. The spin-coated Ag ink on the flat blanket was transferred to a roll blanket at a speed of 8 mm/s under a contact pressure of 6 kgf. Then, the transferred Ag ink was patterned using a cliché at a speed of 2 mm/s under a contact pressure of 2 kgf. Finally, the Ag mesh patterns on the roll blanket were printed on a PC substrate at a speed and force of 5 mm/s and 13 kgf, respectively.

As illustrated in Fig. 1 (b), the printed Ag mesh films with a line width of 3, 10, 50, and 100 μm, respectively, were designed to have 95% optical transmittance by controlling the space between lines. The optical transmittance of printed Ag mesh can be calculated from the opening ratio (OR) as follows [13]:

$$OR = \frac{s^2}{(w+s)^2} \tag{1}$$

$$T_{Ag\ mesh}[\%] = OR \times 100 \tag{2}$$

where, w is line width and s is space, as shown in Fig. 1 (b). The optical transmittance including the substrate can be obtained by multiplying the transmittance of substrate and Ag mesh together:

$$T_{Total}[\%] = T_{substrate}[\%] \times T_{Ag\ mesh}[\%] \div 100 \tag{3}$$

Fig. 1 (c) shows images of Ag mesh films with different line widths. The sample size was 40 × 40 mm^2 and the thickness of the Ag layer was fixed at 300 nm through the same coating process. The optical properties of printed Ag mesh TCEs are summarized in Table 1 with respect to print dimension. The printed Ag mesh films were dried at 130 °C for 10 min using a hot plate to evaporate the solvent of Ag ink.

2.2. Flash light sintering

Flash light sintering was conducted on the reverse-offset printed Ag mesh films using a photonic curing system (PulseForge 1300, Novacentrix Co.). To optimize the electrical and optical properties of Ag mesh films for the printed TCEs, single-pulsed irradiation energy was varied from 3 to 21 J/cm^2, which was measured using a bolometer.

Table 1
Optical properties of printed Ag mesh film with respect to print dimensions.

Print dimension	Linewidth (μm)	3	10	50	100
	Space (μm)	120	400	2000	4000
	Thickness (μm)	0.3	0.3	0.3	0.3
Optical properties	Opening ratio (OR)	0.95	0.95	0.95	0.95
	Fraction of Ag area (1-OR)	0.5	0.5	0.5	0.5
	Measured transmittance (%) including substrate before sintering	85.6	85.5	85.7	85.8
	Bare PC film	90.3% transmittance, 0.22% Haze			
	Measured haze before sintering (%)	1.8	0.78	0.42	0.31

Table 2
Material properties of Ag and PC film used in the heat transfer model.

	Ag	PC
Mass density (g/cm^3)	10.49	1.20
Thermal conductivity (W/m·K)	429	0.22
Specific heat (J/g·°C)	0.240	1.30

The duration time of single-pulse was fixed for 5 ms. Two-step flash light sintering was also employed to reduce the microstructural defects of finely-printed Ag mesh films and substrate degradations. This was divided into the following two pathways: 1) the preheating step, which is composed of multi-pulses, and 2) the main sintering step, which is composed of a single pulse. In the preheating step, the multi-pulsed flash light with a pulse duration time of 100 μs and a pulse turn-off time of 100 μs was irradiated on the printed TCEs. The total irradiation energy of 5 J/cm^2 was divided into multi-pulses, which was varied 5 to 20 times. After the preheating step, a single-pulsed flash light of 5 J/cm^2 was irradiated on the TCEs for 1 ms as the main sintering step.

2.3. Characterization of flash light-sintered TCEs

We measured the sheet resistances and optical transmittance of flash light-sintered Ag mesh TCEs using an eddy current probe measurement system (EC-80P, Napson Co.) and a UV–visible spectrophotometer (Lambda 750 s, Perkin elmer Co.), respectively. The optical haze value, including the substrate, was evaluated by a hazemeter (HM-150L2, Murakamilab Co.). The microstructural development was analyzed using an optical microscope (OptelicsC130, Lasertec Co.) and a field-emission scanning electron microscope (FE-SEM, Magellan400, FEI Co.). The cross-sectional SEM images of the sintered Ag mesh films were acquired using a focus ion beam (FIB, Helios Nanolab 450 F1, FEI Co.).

2.4. Temperature calculation using a 2-D heat transfer model

We employed commercial finite element analysis software (Abaqus, Dassault system Co.) to calculate the rise in temperature depending on the printed line width during flash light sintering. In this calculation, the 2-D cross-section of Ag lines on a PC substrate was depicted in a square of 400 × 400 μm^2 based on the actual size of printed Ag lines, as shown in Table 1. Uniform meshes of 0.1 and 1 μm in size were generated for

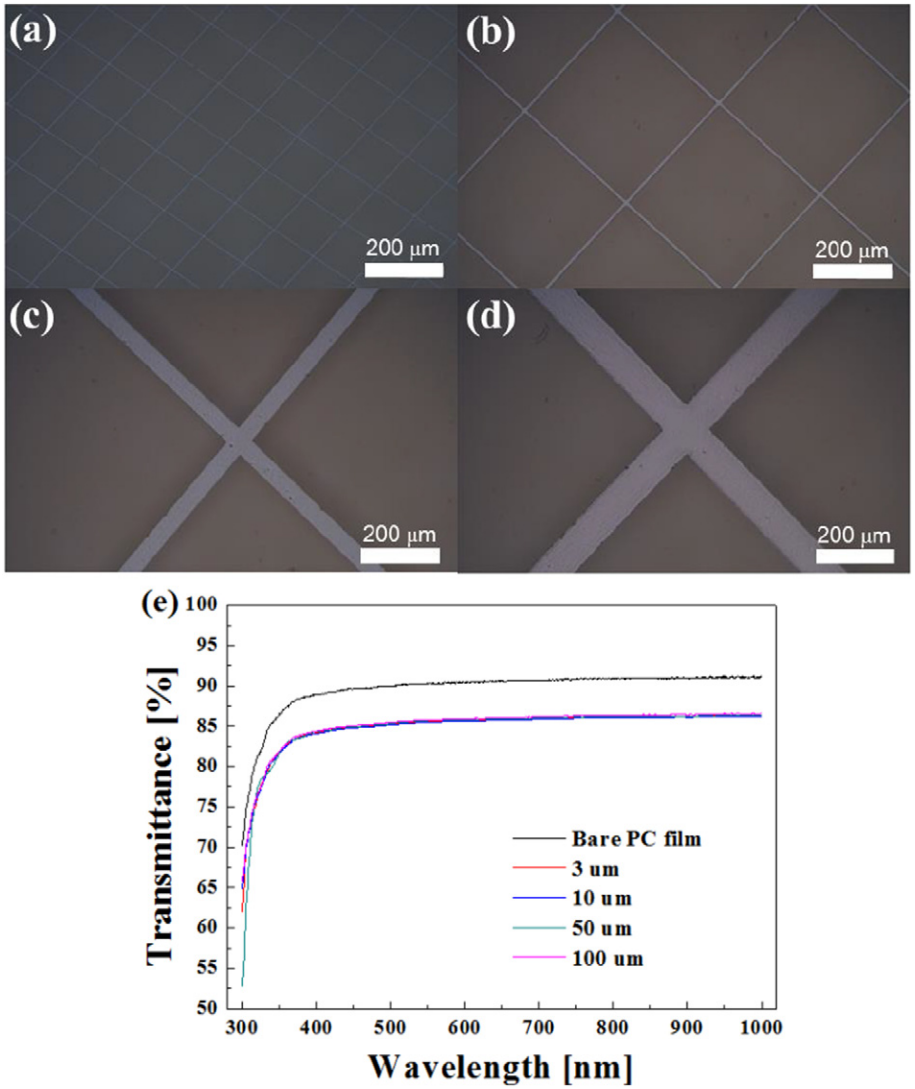

Fig. 2. Optical microscopy images of printed Ag mesh film with a line width of: (a) 3 μm, (b) 10 μm, (c) 50 μm and (d) 100 μm before flash light sintering; and (e) their optical transmittance.

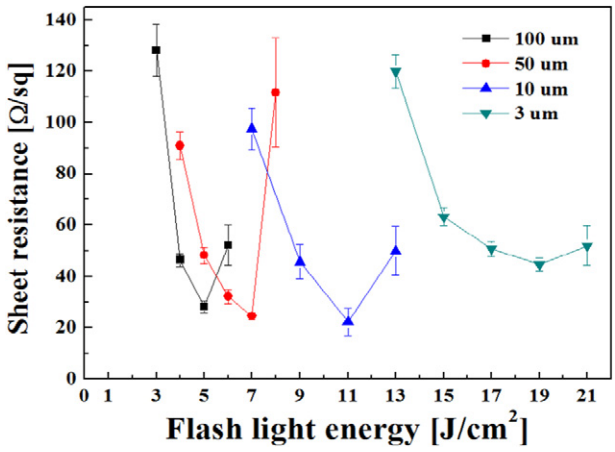

Fig. 3. Sheet resistance changes of flash light-sintered Ag mesh film with respect to flash light energy and line width.

the Ag lines and the PC substrate, respectively, and their interfaces were perfectly attached to each other. For the simulation of flash light irradiation, it is assumed that irradiation energy is converted into heat on top of the printed Ag line. The transient heat transfer from the top surface to the printed line and to the substrate can be described as follows:

$$\rho C_p \frac{\partial T}{\partial t} = \nabla\cdot(k\nabla T) + Q \tag{4}$$

where, ρ is density, C_p is specific heat capacity, T is temperature, k is thermal conductivity, and Q is internal heat generation. In this transient temperature analysis, the constant thermal properties of Ag and PC were used, as shown in Table 2. The boundary condition of surfaces exposed to air is described as:

$$k\frac{\Delta T}{\Delta n} = -h(T_s - T_\infty) \tag{5}$$

where, n is the normal vector to the surface, h is the convection coefficient of the surface, T_s is the surface temperature, and T_∞ is the atmosphere temperature. In this calculation, the convention coefficient h is 30 $W/m^2\cdot K$. From this analysis, the temperature changes of the printed Ag layer and PC substrate and their images were extracted as a function of sintering time and line width.

3. Results and discussion

The optical microscopy images in Fig. 2 (a–d) show that the Ag mesh patterns with different line widths of 3, 10, 50, and 100 μm were clearly printed on the polymer substrates without printing defects or stains. The thickness of each pattern was 0.3 μm, as summarized in Table 1, which was controlled by maintaining the same printing procedures. The opening ratio (OR) of each pattern was designed to have 0.95 using Eq. (1). Thus, the fractions of Ag line areas (1-OR) were also fixed with 0.5, as summarized in Table 1. The OR is directly connected to the optical transmittance of mesh patterns, as shown in Eqs. (1)–(3). Therefore, we measured the optical transmittance of

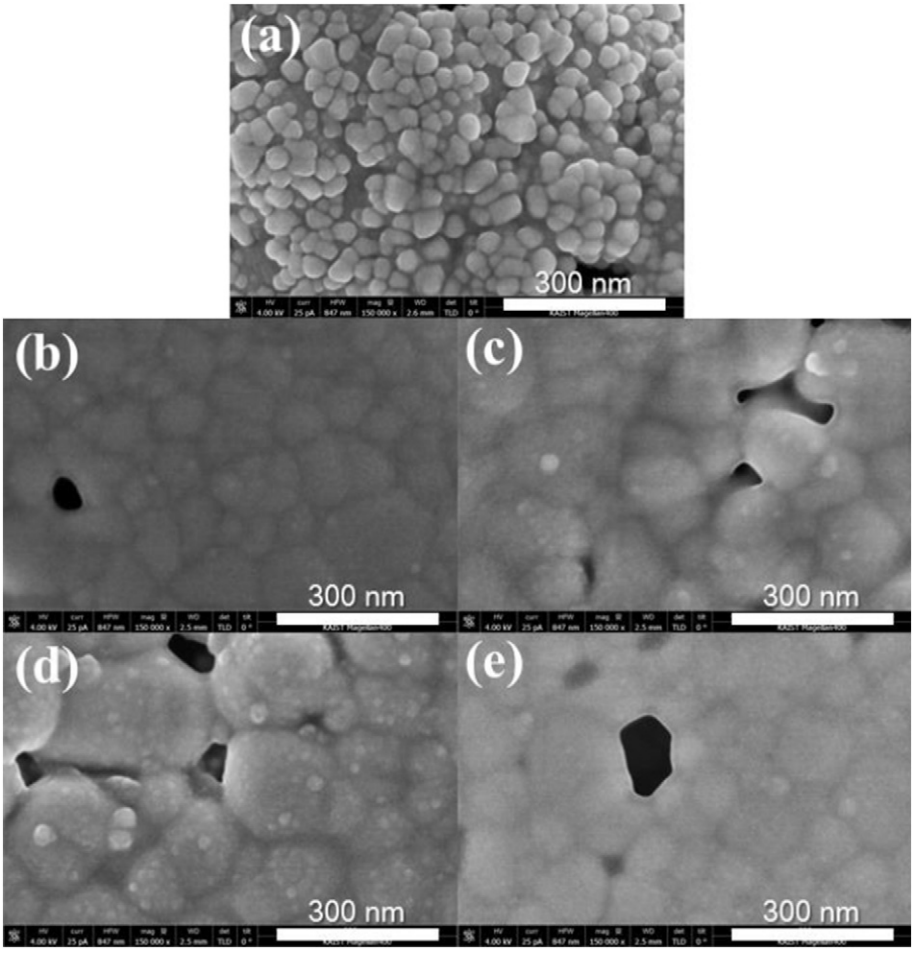

Fig. 4. SEM images of (a) as-dried and (b-e) flash light-sintered Ag mesh film demonstrating the lowest sheet resistance, as shown in Fig. 3. The optimal flash light energy depending on the line width is as follows: (b) 19 J/cm^2 for 3 μm (c) 11 J/cm^2 for 10 μm, (d) 7 J/cm^2 for 50 μm, and (e) 5 J/cm^2 for 100 μm.

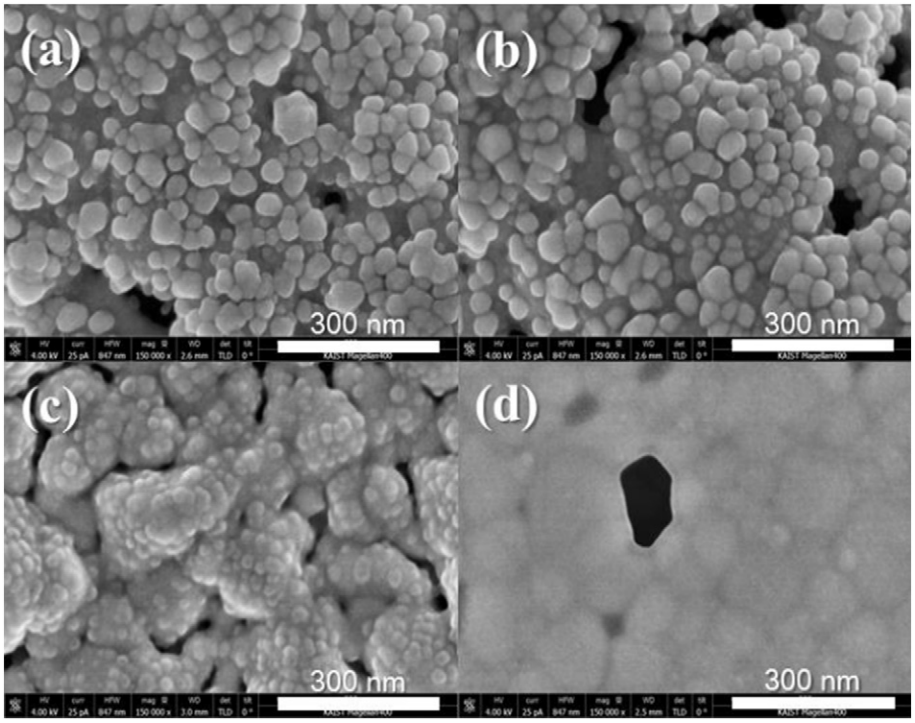

Fig. 5. SEM images of Ag mesh film sintered with an identical flash light irradiation energy of 5 J/cm^2: (a) 3 μm, (b) 10 μm, (c) 50 μm, and (d) 100 μm.

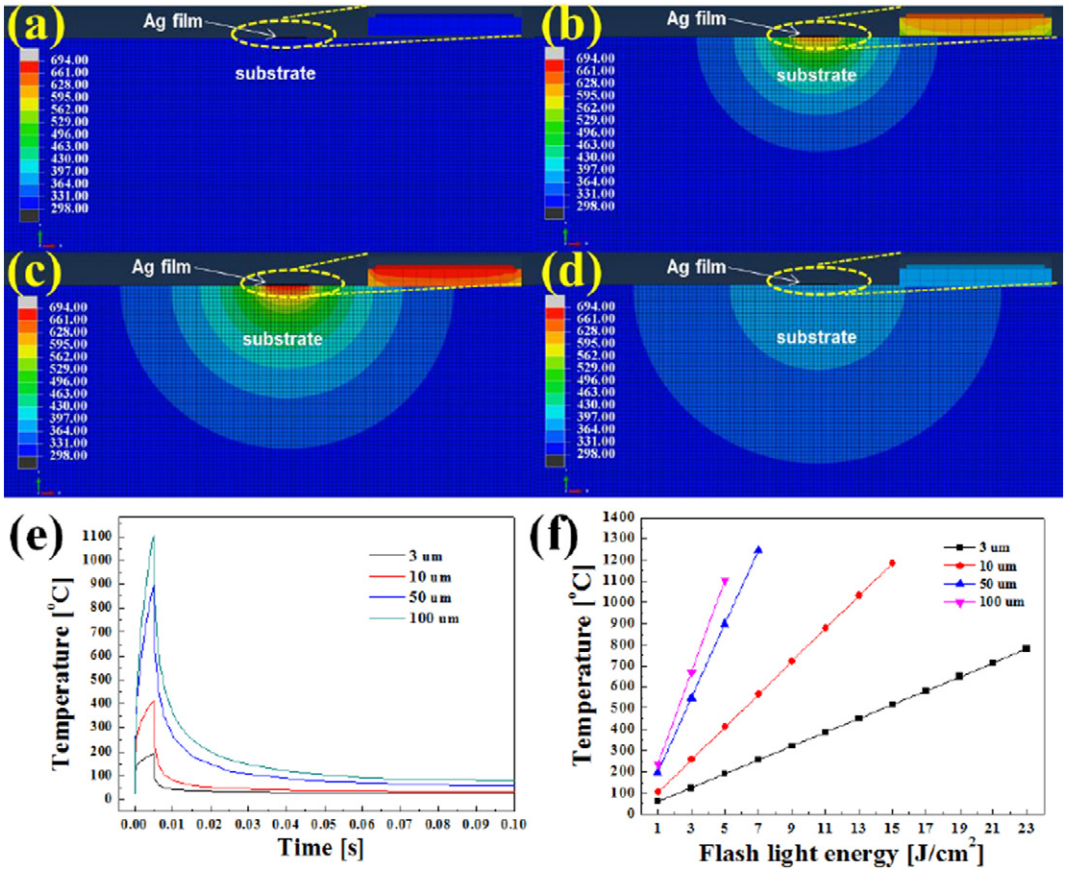

Fig. 6. The visualized temperature distribution of a 10-μm wide Ag line with a sintering time of: (a) 0 ms, (b) 2.5 ms, (c) 5 ms, and (d) 7.5 ms (Expanded images of the Ag layer are shown in the inset images). (e) Calculated temperature in the Ag layers with respect to sintering time and line width when a single-pulsed flash light was irradiated with a pulse duration time of 5 ms and a light energy of 5 J/cm^2. (f) Maximum peak temperature of a flash light-sintered Ag layer with respect to light energy and line width.

printed Ag mesh patterns before sintering as shown in Fig. 2 (e). All of the Ag mesh film had the same optical transparency of 85.7% at 550 nm including 90.3% optical transmittance of PC substrate, which proves that the ORs are the same regardless of line width. Thus, the amount of printed Ag ink is also the same, regardless of line width.

Flash light sintering was conducted on the printed Ag mesh films. A single and rectangular pulsed flash light was irradiated on the films for a pulse duration time of 5 ms. To obtain the lowest sheet resistance of the printed TCEs, the flash light energy was varied from 3 to 21 J/cm^2. Fig. 3 shows the sheet resistances of flash light-sintered Ag mesh films with respect to flash light energy. When the flash light energy was increased, the sheet resistance of each film drastically decreased and then increased again. It is also worth noting that the flash light energy for the lowest sheet resistance increased when line width decreased. Thus, the optimal energy conditions for 3, 10, 50, and 100 μm-wide lines were 19, 11, 7, and 5 J/cm^2, respectively. The rupture or burning of Ag mesh films appeared above these energies due to the excessive energy, which led to the increase of sheet resistance. These sintering results were never observed in thermally sintered silver mesh TCEs [37].

The SEM images in Fig. 4 show the microstructures of flash light-sintered Ag mesh films having the lowest sheet resistance in Fig. 3. In as-dried film that is shown in Fig. 4 (a), Ag nanoparticles with a size of 30–60 nm were agglomerated each other. The flash light-sintered Ag mesh films shown in Fig. 4 (b–e) reveal a similar densified microstructure with a grain growth above ~100 nm, which can effectively reduce electrical resistivity. These images clearly reveal that the different irradiation energies of 19, 11, 7, and 5 J/cm^2 induce a similar sintering microstructure. On the other hand, after flash light sintering with the same irradiation energy of 5 J/cm^2, each Ag film with a different line width of 3, 10, 50, and 100 μm showed a different microstructural development. Ag films with a narrower line width (Fig. 5 (a–b)) have small nanoparticles with a grain size of 30–60 nm, which is similar to the microstructure of as-dried state of printed Ag mesh film (Fig. 4 (a)). When the line width was increased to 50 μm, the Ag nanoparticles merged with each other (Fig. 5 (c)), and then a denser grain growth of 60–150 nm was observed in the Ag film with a line width of 100 μm (Fig. 5 (d)). As shown in Fig. 3, the Ag mesh films in Fig. 5 (a–b) showed a sheet resistance of several MΩ/□ or kΩ/□, which were out of

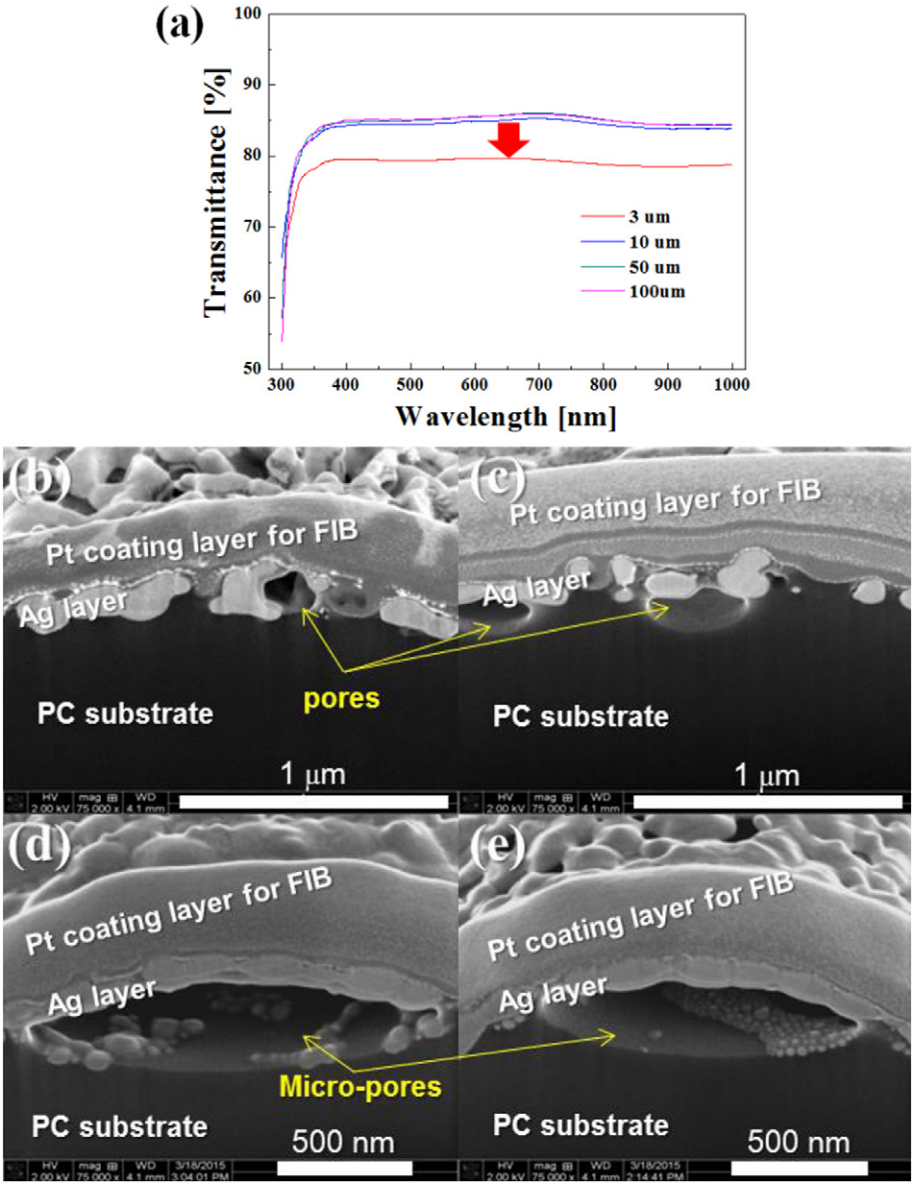

Fig. 7. (a) Optical transmittance of Ag mesh film with the lowest sheet resistance, as shown in Fig. 3. The cross-sectional SEM images of 3-μm wide Ag lines light-sintered with a pulse duration time of 5 ms and a light energy of (b) 15 J/cm^2, (c) 17 J/cm^2, (d) 19 J/cm^2, and (e) 21 J/cm^2.

measurable range. Only the Ag mesh films in Fig. 5(c–d) had a sheet resistance of 48.3 Ω/□ and 28.2 Ω/□, respectively. These results clearly reveal that the same energy of flash light irradiation induces completely different microstructural development and electrical properties even though the same Ag ink and amount were printed regardless of line width.

During flash light sintering, metal nanoparticles can absorb visible light via plasmonic resonance and this absorbed light energy will be converted to thermal energy, which drives the sintering of metal nanoparticles [20,26,29,35]. In our study, even though the same Ag ink was used and the same amount of it was printed on substrates, the sintering progress was completely different. Therefore, we focused on the heat conduction process. The converted thermal energy will either be conducted into the inside of Ag film and then into substrate or it will dissipate into the air. During this heat conduction or heat dissipation process, the print dimensions can influence the release of thermal energy due to the different surface-to-volume ratios. Thus, transient heat transfer analysis was conducted in order to calculate the temperature of the printed Ag mesh films. As explained in experimental procedures, for the simulation of flash light irradiation, it is assumed that irradiation energy is converted into heat on top of the printed Ag line. There were two pathways of heat dissipation. One is from the Ag film into a substrate and the other is from Ag film into the air. Because the narrower line width has a relatively larger heat dissipation area, the calculated temperature inside of the Ag film explains how print dimensions can affect the flash light sintering of Ag mesh film.

Fig. 6 (a–d) show the changes in temperature distribution in a 10-μm wide Ag line when a single and rectangular pulsed light with a duration time of 5 ms and a light energy of 5 J/cm^2 is irradiated. The temperature distribution images with the sintering time clearly show that the Ag layer is heated up to 390 °C during sintering and that the heat simultaneously dissipates into the PC substrate. At 7.5 ms, right after the sintering process is carried out, the temperature of ~90 °C remains in the Ag layer and the PC substrate, as shown in Fig. 6 (d). Temperature changes in the Ag layer are given in Fig. 6 (e) with respect to sintering time. The temperature of the Ag layer instantly rises to the maximum peak value and then

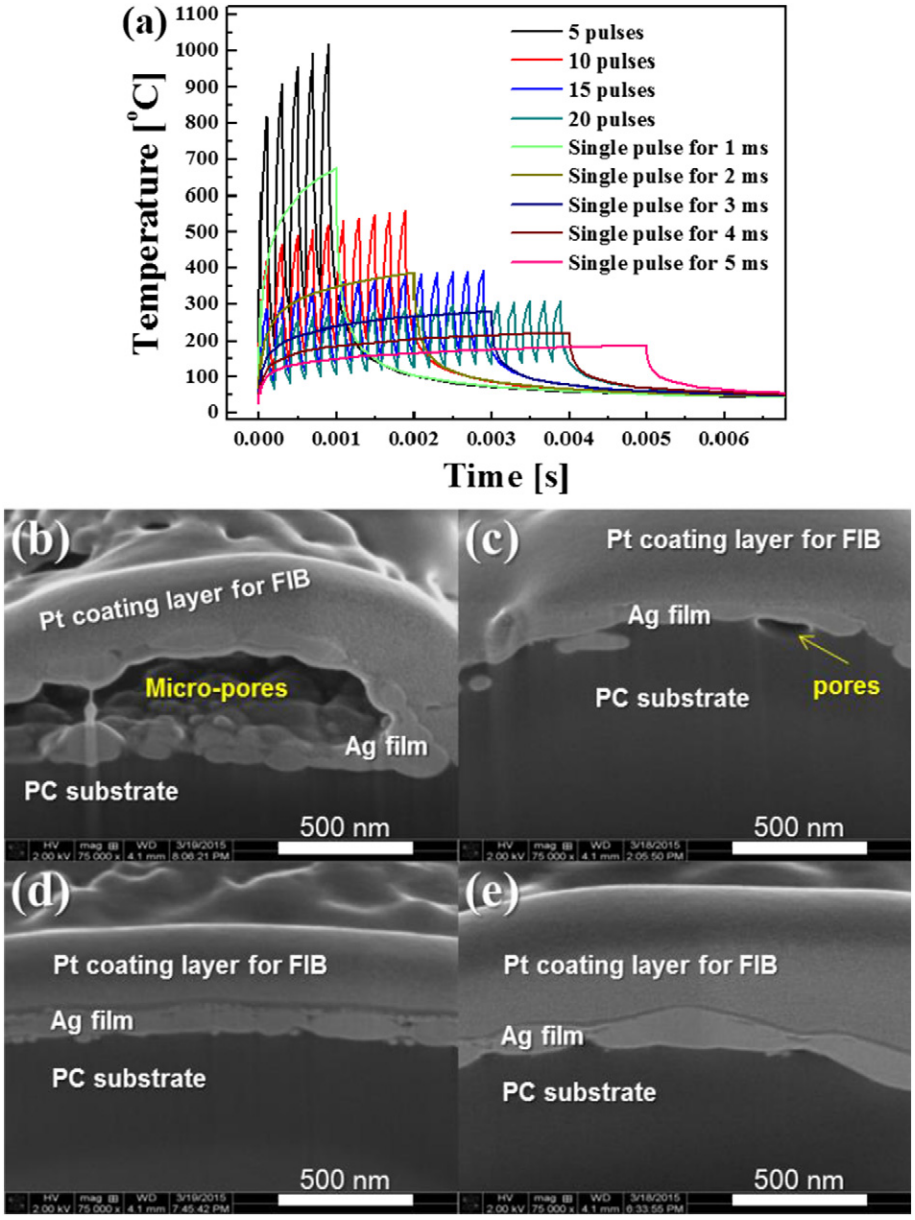

Fig. 8. (a) Calculated temperature of 3-μm wide Ag lines with respect to pulse numbers and pulse duration time, and the cross-sectional SEM images of the Ag lines treated with the two-step flash light sintering method. A preheating step composed of (b) 5 pulses, (c) 10 pulses, (d) 15 pulses or (f) 20 pulses, and a main sintering step with a single rectangular pulse of 5 J/cm^2 for 1 ms was consecutively conducted.

abruptly decreases after the sintering. When the Ag line width was decreased from 100 to 3 μm, the maximum peak temperature decreased from 1100 to 180 °C and the residual heat decreased from 100 °C to room temperature. This temperature decrease with the decrease in line width well explains the different microstructural development and resulting electrical properties after the same flash light sintering was conducted as shown in Figs. 3 and 5. Fig. 6 (f) provides a summary of the changes in maximum peak temperature with respect to flash light energy and line width. The temperature inside of the Ag films linearly increased with the increase of the line width as well as flash light energy even though the surface of Ag films absorbed the same amount of flash light energy.

Fig. 7 (a) shows the optical transmittance of flash light-sintered Ag mesh films that show the lowest sheet resistance, as presented in Fig. 3. Each Ag mesh film was sintered with a different flash light energy depending on the line width as follows: 19 J/cm^2 for 3 μm, 11 J/cm^2 for 10 μm, 7 J/cm^2 for 50 μm, and 5 J/cm^2 for 100 μm. The Ag mesh films with a line width of 10 to 100 μm showed an optical transmittance of 85.0%; whereas, the optical transmittance of an Ag mesh film with a line width of 3 μm was lowered to 79.5%, as indicated with a red arrow in Fig. 7 (a). The lowest sheet resistance of 3 μm wide Ag mesh patterns in Fig. 3 was much higher than that of other mesh patterns.

To investigate the main reasons why the electrical and optical properties of 3 μm wide Ag mesh patterns were deteriorated, the cross-sectional microstructure of Ag mesh film was analyzed using a FIB-equipped SEM, which is presented in Fig. 7 (b–f). The SEM images of Fig. 7 (b) and (c) clearly reveal that small pores are generated at the interface between Ag film and PC substrate when the films are sintered with lower energy. These defects developed into the micro-pores or delamination of the Ag layer with the increase of flash light energy, as shown in Fig. 7 (d) and (f). When the surface sintering was faster than the interior sintering due to higher energy irradiation, the evaporated organic materials trapped in the films could generate these interfacial defects. The Ag mesh films with a line width of 3 μm required three or four times higher flash light energy for obtaining the lowest sheet resistance, which was much higher than that of Ag mesh film with a greater line width as explained in Fig. 3. Since 3-μm-wide lines have a lower temperature rise, in spite of having a higher irradiation energy, a much higher heat dissipation from the Ag layer to the PC substrate should induce the thermal degradation of the PC substrate near the Ag lines, which can affect the optical transmittance of substrate. Moreover, Ag mesh film with narrower lines has a higher mesh density. This results in a larger degraded substrate area.

As a means of reducing irradiation energy and interfacial defects, multi-pulses were applied to flash light sintering. Fig. 8 (a) shows the calculated temperature rise when the flash light energy of 5 J/cm^2 is irradiated with a form of single-pulsed or multi-pulsed light. When the duration time decreases from 5 to 1 ms, the temperature rise in 3-μm-wide Ag lines can only be increased from 189 to 677 °C with the irradiation energy of 5 J/cm^2. The effective temperature rise with lower irradiation energy can mitigate the dissipation energy to the substrate. Thus, when the Ag mesh films were sintered with a single-pulsed light of 5 J/cm^2 for 1 ms, the deterioration of optical transmittance was improved in comparison with the optical transmittance of Fig. 7 (a). However, the micro-pore or the delamination of the Ag layer was still observed and the sheet resistance was not optimized with a value of 83 Ω/□.

To optimize sheet resistance by removing interfacial defects, a preheating step composed of multi-pulses (Fig. 8 (a)) was introduced before the main sintering was carried out with a single-pulsed light of 5 J/cm^2 for 1 ms in order to effectively evaporate any organic residue. Multi-pulsed irradiation can provide a resting time in the temperature rise intervals, during which the evaporated organic residue can be released before the surface sintering completely progressed. Figs. 8 (b–f) show a cross-sectional view of two-step sintered Ag mesh films with a line width of 3 μm. After being preheated with 5 pulses, micro-pores were still observed, as shown in Fig. 8 (b). However, as the pulse number increases, defects, such as delamination or micro-pores, gradually disappear, and then the defects completely disappear above 15 pulses, as indicated in Fig. 8 (d–e).

As a result, the preheating temperature should be high enough to vaporize the organic residue but low enough to suppress the surface sintering. Thus, most of the preheating conditions did not show any electrical conductance, except for 5-pulsed irradiation, which had a sheet resistance of 823 Ω/□. However, it increased to 4 kΩ/□ after the main sintering step was executed, as shown in Fig. 9 (a). Fig. 9 (a) also shows the sheet resistance changes in Ag mesh films in regards to the pulse number after two-step sintering. When the pulse number was increased from 5 to 15 pulses, the sheet resistance decreased to 27 Ω/□ and then increased to 57 Ω/□. The microstructural and electrical analyses clearly indicate that 15 pulses are optimum for the preheating step. Fig. 9 (b) shows the optical transmittance of Ag mesh films with a line width of 3 μm after the optimized two-step flash light sintering was carried out. The Ag mesh film showed an optical transmittance of 84.7% at 550 nm, which means that the substrate damage for finely-printed Ag lines can be effectively controlled by optimizing the flash light sintering process.

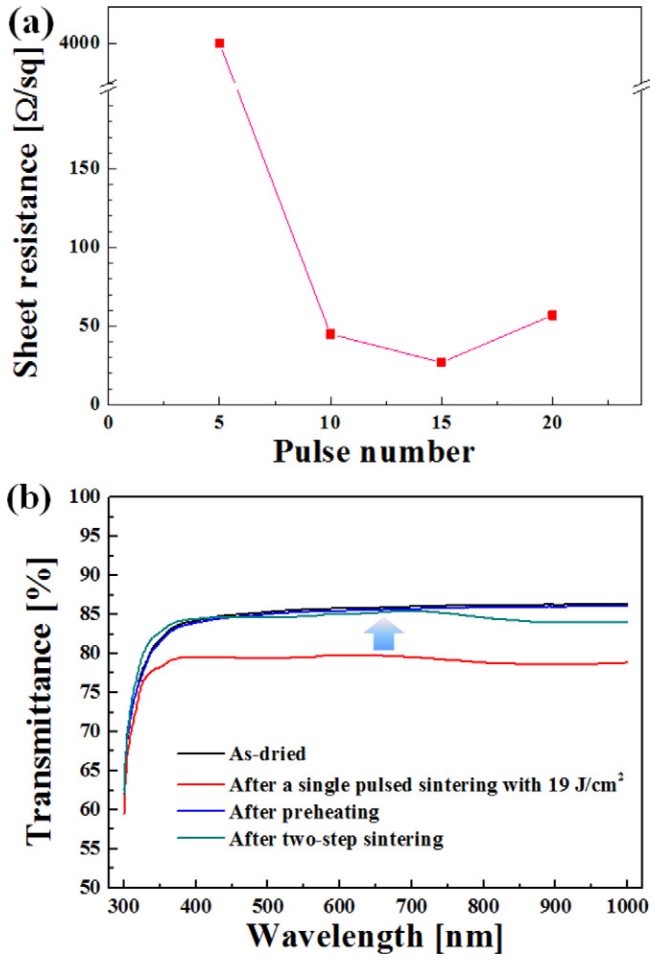

Fig. 9. (a) Sheet resistance changes of flash light-sintered Ag mesh film with a line width of 3 μm and (b) the optical transmittance of Ag mesh film with a line width of 3 μm via the two-step flash light sintering process.

4. Conclusions

In this study, we carried out flash light sintering on printed Ag mesh films to fabricate flexible transparent conducting films. The print dimensions, such as line width, influenced the sintering progress even

though the same Ag ink was used. The narrower printing line requires a higher flash light energy to obtain an equivalent sheet resistance. Microstructural development was also retarded with the decrease of line width for the same flash light energy. These results suggest that the temperature rise in each film could vary depending on print dimensions. Additionally, the transient heat transfer analysis revealed that the temperature of the Ag films decreased with the decrease of line width for the same flash light energy because the print dimensions influenced the dissipation or release of thermal energy. The Ag mesh film with a line width of 3 μm required much higher flash light energy, which induced the deterioration of optical transmittance and interfacial defects. By employing two-step flash light sintering, the printed Ag mesh TCEs with 3-μm-wide lines had a sheet resistance of 27 Ω/□ and an optical transmittance of 84.7%.

Acknowledgements

This research has been financially supported by the Government-funded Research Program of the Korea Institute of Machinery and Materials (Grant NK194C) and the R&D Convergence Program of the National Research Council for Science and Technology for the Republic of Korea (CAP-15-04-KITECH).

References

[1] Y.B. Park, L. Hu, G. Gruner, G. Irvin, P. Drzaic, 37.4: Late-News Paper: Integration of Carbon Nanotube Transparent Electrodes into Display Applications, SID Symposium Digest of Technical Papers, Wiley Online Library, 2008 537–540.
[2] A. Schindler, J. Brill, N. Fruehauf, J.P. Novak, Z. Yaniv, Solution-deposited carbon nanotube layers for flexible display applications, Physica E: Low-Dimensional Systems and Nanostructures 37 (2007) 119–123.
[3] D.S. Hecht, D. Thomas, L. Hu, C. Ladous, T. Lam, Y. Park, G. Irvin, P. Drzaic, Carbon-nanotube film on plastic as transparent electrode for resistive touch screens, J. Soc. Inf. Disp. 17 (2009) 941–946.
[4] J. Lee, P. Lee, H. Lee, D. Lee, S.S. Lee, S.H. Ko, Very long Ag nanowire synthesis and its application in a highly transparent, conductive and flexible metal electrode touch panel, Nano 4 (2012) 6408–6414.
[5] S. Choi, Y. Zhou, W. Haske, J.W. Shim, C. Fuentes-Hernandez, B. Kippelen, ITO-free large-area flexible organic solar cells with an embedded metal grid, Org. Electron. 17 (2015) 349–354.
[6] J.-S. Yu, I. Kim, J.-S. Kim, J. Jo, T.T. Larsen-Olsen, R.R. Søndergaard, M. Hösel, D. Angmo, M. Jørgensen, F.C. Krebs, Silver front electrode grids for ITO-free all printed polymer solar cells with embedded and raised topographies, prepared by thermal imprint, flexographic and inkjet roll-to-roll processes, Nano 4 (2012) 6032–6040.
[7] J. Chae, S. Appasamy, K. Jain, Patterning of indium tin oxide by projection photoablation and lift-off process for fabrication of flat-panel displays, Appl. Phys. Lett. 90 (2007) 261102.
[8] H. Löbl, M. Huppertz, D. Mergel, ITO films for antireflective and antistatic tube coatings prepared by dc magnetron sputtering, Surf. Coat. Technol. 82 (1996) 90–98.
[9] D.R. Cairns, R.P. Witte II, D.K. Sparacin, S.M. Sachsman, D.C. Paine, G.P. Crawford, R. Newton, Strain-dependent electrical resistance of tin-doped indium oxide on polymer substrates, Appl. Phys. Lett. 76 (2000) 1425–1427.
[10] D.R. Cairns, G.P. Crawford, Electromechanical properties of transparent conducting substrates for flexible electronic displays, Proc. IEEE 93 (2005) 1451–1458.
[11] J.-S. Yu, J. Jo, S.-M. Yoon, D.-J. Kim, Fabrication of transparent conductive electrode film using thermal roll-imprinted ag metal grid and coated conductive polymer, J. Nanosci. Nanotechnol. 12 (2012) 1179–1182.
[12] Y. Jang, J. Kim, D. Byun, Invisible metal-grid tansparent electrode prepared by electrohydrodynamic (EHD) jet printing, J. Phys. D. Appl. Phys. 46 (2013) 155103 (5pp).
[13] J. Hautcoeur, X. Castel, F. Colombel, R. Benzerga, M. Himdi, G. Legeay, E. Motta-Cruz, Transparency and electrical properties of meshed metal films, Thin Solid Films 519 (2011) 3851–3858.
[14] D. Ghosh, T. Chen, V. Pruneri, High figure-of-merit ultrathin metal transparent electrodes incorporating a conductive grid, Appl. Phys. Lett. 96 (2010) 041109.
[15] S. De, T.M. Higgins, P.E. Lyons, E.M. Doherty, P.N. Nirmalraj, W.J. Blau, J.J. Boland, J.N. Coleman, Silver nanowire networks as flexible, transparent, conducting films: extremely high DC to optical conductivity ratios, ACS Nano 3 (2009) 1767–1774.
[16] J. Wu, H.A. Becerril, Z. Bao, Z. Liu, Y. Chen, P. Peumans, Organic solar cells with solution-processed graphene transparent electrodes, Appl. Phys. Lett. 92 (2008) 263302.
[17] M.W. Rowell, M.A. Topinka, M.D. McGehee, H.-J. Prall, G. Dennler, N.S. Sariciftci, L. Hu, G. Gruner, Organic solar cells with carbon nanotube network electrodes, Appl. Phys. Lett. 88 (2006) 233506.
[18] K.-S. Chou, K.-C. Huang, H.-H. Lee, Fabrication and sintering effect on the morphologies and conductivity of nano-Ag particle films by the spin coating method, Nanotechnology 16 (2005) 779.
[19] E. Halonen, T. Viiru, K. Ostman, A.L. Cabezas, M. Mantysalo, Oven sintering process optimization for inkjet-printed Ag nanoparticle ink, IEEE Transactions on Components, Packaging and Manufacturing Technology 3 (2013) 350–356.
[20] H.-S. Kim, S.R. Dhage, D.-E. Shim, H.T. Hahn, Intense pulsed light sintering of copper nanoink for printed electronics, Applied Physics A 97 (2009) 791–798.
[21] H.-J. Hwang, W.-H. Chung, H.-S. Kim, In situ monitoring of flash-light sintering of copper nanoparticle ink for printed electronics, Nanotechnology 23 (2012) 485205.
[22] W.-H. Chung, H.-J. Hwang, S.-H. Lee, H.-S. Kim, In situ monitoring of a flash light sintering process using silver nano-ink for producing flexible electronics, Nanotechnology 24 (2012) 035202.
[23] S.-H. Park, S. Jang, D.-J. Lee, J. Oh, H.-S. Kim, Two-step flash light sintering process for crack-free inkjet-printed Ag films, J. Micromech. Microeng. 23 (2012) 015013.
[24] S.-H. Park, H.-S. Kim, Flash light sintering of nickel nanoparticles for printed electronics, Thin Solid Films 550 (2014) 575–581.
[25] S.-J. Joo, S.-H. Park, C.-J. Moon, H.-S. Kim, A highly reliable copper nanowire/nanoparticle ink pattern with high conductivity on flexible substrate prepared via a flash light-sintering technique, ACS Appl. Mater. Interfaces 7 (2015) 5674–5684.
[26] H.-J. Hwang, K.-H. Oh, H.-S. Kim, All-photonic drying and sintering process via flash white light combined with deep-UV and near-infrared irradiation for highly conductive copper nano-ink, Sci. Report. 6 (2016).
[27] E.-B. Jeon, S.-J. Joo, H. Ahn, H.-S. Kim, Two-step flash light sintering process for enhanced adhesion between copper complex ion/silane ink and a flexible substrate, Thin Solid Films 603 (2016) 382–390.
[28] C.-H. Ryu, S.-J. Joo, H.-S. Kim, Two-step flash light sintering of copper nanoparticle ink to remove substrate warping, Appl. Surf. Sci. (2016) DOI.
[29] J. Jiu, T. Sugahara, M. Nogi, T. Araki, K. Suganuma, H. Uchida, K. Shinozaki, High-intensity pulse light sintering of silver nanowire transparent films on polymer substrates: the effect of the thermal properties of substrates on the performance of silver films, Nano 5 (2013) 11820–11828.
[30] J. Perelaer, R. Abbel, S. Wünscher, R. Jani, T. van Lammeren, U.S. Schubert, Roll-to-roll compatible sintering of inkjet printed features by photonic and microwave exposure: from non-conductive ink to 40% bulk silver conductivity in less than 15 seconds, Adv. Mater. 24 (2012) 2620–2625.
[31] D. Angmo, T.T. Larsen-Olsen, M. Jørgensen, R.R. Søndergaard, F.C. Krebs, Roll-to-roll inkjet printing and photonic sintering of electrodes for ITO free polymer solar cell modules and facile product integration, Adv. Energy Mater. 3 (2013) 172–175.
[32] M. Hösel, F.C. Krebs, Large-scale roll-to-roll photonic sintering of flexo printed silver nanoparticle electrodes, J. Mater. Chem. 22 (2012) 15683–15688.
[33] J. Niittynen, R. Abbel, M. Mäntysalo, J. Perelaer, U.S. Schubert, D. Lupo, Alternative sintering methods compared to conventional thermal sintering for inkjet printed silver nanoparticle ink, Thin Solid Films 556 (2014) 452–459.
[34] J. Ryu, H.-S. Kim, H.T. Hahn, Reactive sintering of copper nanoparticles using intense pulsed light for printed electronics, J. Electron. Mater. 40 (2011) 42–50.
[35] Y.-T. Hwang, W.-H. Chung, Y.-R. Jang, H.-S. Kim, Intensive Plasmonic flash light sintering of copper nanoinks using a band-pass light filter for highly electrically conductive electrodes in printed electronics, ACS Appl. Mater. Interfaces 8 (2016) 8591–8599.
[36] S.-H. Park, W.-H. Chung, H.-S. Kim, Temperature changes of copper nanoparticle ink during flash light sintering, J. Mater. Process. Technol. 214 (2014) 2730–2738.
[37] I. Kim, S.-W. Kwak, Y. Ju, G.-Y. Park, T.-M. Lee, Y. Jang, Y.-M. Choi, D. Kang, Roll-offset printed transparent conducting electrode for organic solar cells, Thin Solid Films 580 (2015) 21–28.